A discrete Funk transform on the Cubed Sphere

Jean-Baptiste Bellet

A DISCRETE FUNK TRANSFORM ON THE CUBED SPHERE

JEAN-BAPTISTE BELLET

Abstract. Computing accurately Funk transforms from discrete values is crucial in some applications, such as Q-Ball Imaging in medicine. This paper deals with a new discrete Funk transform devoted to such computation, in the case of a hemispherical grid extracted from the Cubed Sphere with step $\pi/(2N)$. The approach is based on a spectral method applied on a least squares fitting, in the space of even spherical harmonics with degree at most $2N-2$. We prove various properties satisfied by the new transform, including an analogous description of the pseudoinverse. Remarkably, the transform and the pseudoinverse are expected to be stable, despite the least square fitting is not regularized. Numerical results attest to the accuracy and the stability, in particular for synthetic Gaussian signals from Q-Ball Imaging.

1. Introduction

The Funk transform from [14], also called the Funk-Minkowski transform, the Funk-Radon transform, or the spherical Radon transform, is an integral transform which averages a function along great circles on the unit sphere $\mathbb{S}^2$. This transform, similar integral transforms, and associated inverse problems, are the subject of many mathematical studies, such as [17,23,25,32,37] and the references therein. These transforms play an important role in various applications, including photoacoustic tomography [18,44], Synthetic Aperture Radar [43] and diffusion Magnetic Resonance Imaging (dMRI) [20,41].

To specify one successful example from medicine, *Q-Ball Imaging* images the orientation of fibers in biological tissues [41]. The key step of this method computes the Funk transform of dMRI signals recorded on discrete grids. The original computation [41] is a trapezoidal quadrature rule, applied on an interpolating function. The numerical scheme has been improved in [12], using a spectral method on a regularized least squares approximation. The huge success[1] of the articles [12,41] attests that it is crucial to master the Funk transform in discrete configurations.

In this paper, we focus on a discretization of the Funk transform, assuming that the considered spherical grid is the equiangular Cubed Sphere. This Cubed Sphere (and other ones) are well known in numerical climatology and meteorology [26, 28–30, 33–35, 38]. A wide variety of numerical methods has been successfully adapted to Cubed Sphere grids, *e.g.* in [8–10, 13, 19, 21, 22, 24, 27, 31, 36, 39, 42] and the references therein. Nevertheless, to the author's knowledge, the Funk transform has never been tested on Cubed Spheres, whereas they are natural candidates to define an accurate discrete Funk transform, due to interesting properties such as quasi-uniformity. This is the initial motivation of this study.

This paper is also part of a series of works dealing with computing on the equiangular Cubed Sphere using spherical harmonics; Lagrange interpolation has been considered in [4], least squares approximation in [6], and a spherical quadrature rule in [5]. These very recent works show that spectral computing on the Cubed Sphere is promising. Here, we continue in this direction for approximating the Funk transform. In a word, we define a new discrete Funk transform, based on the spectral decomposition of the Funk transform, applied on a least squares fitting on the Cubed Sphere. The precise definition is summarized hereafter, with notation and assumption clarified later in the text.

Date: October 18, 2022.

2020 *Mathematics Subject Classification.* 65R10, 44A12, 92C55.

Key words and phrases. Cubed Sphere, least squares, spherical harmonics, Funk transform, Radon transform.

[1]The website of the journal *Magnetic Resonance in Medicine* mentions 1421 citations for [41], and 555 citations for [12], on October 18, 2022.

Definition 1 (Discrete Funk transform)**.** Let $N \geq 1$, and $D = 2N - 2$. Let CH_N be a half of the Cubed Sphere with step $\frac{\pi}{2N}$, defined in (4,6). Let $A = A_N^D$ be the Vandermonde matrix on CH_N of the even spherical harmonics with degree at most D, defined in (9). Let $\Lambda = \Lambda_D$ be the diagonal matrix defined in (3), corresponding to the Funk transform of these spherical harmonics. Assuming that A has full column rank, we define the discrete Funk transform on the grid CH_N as the matrix

$$\mathrm{F} = A\,\Lambda\,(A^\intercal A)^{-1}A^\intercal \in \mathbb{R}^{(3N^2+1)\times(3N^2+1)}. \tag{1}$$

This transform is based on a spectral method very similar with the one from [12]. The new features are the following ones:

(a) the grid is extracted from a Cubed Sphere with step $\frac{\pi}{2N}$;
(b) the approximation space is $\mathcal{Y}_{2N-2}^{\mathrm{ev}} = \mathbb{Y}_0 \oplus \cdots \oplus \mathbb{Y}_{2n} \oplus \cdots \oplus \mathbb{Y}_{2N-2}$;
(c) a least squares fitting is operated without any regularization.

In particular, we claim that (c) is possible in a stable way, due to our particular choice of the grid in (a) and our choice of the approximation space in (b).

In this paper, we explain in details and we motivate Definition 1. This includes the definition of CH_N, which is a new spherical grid that is relevant for manipulating even spherical functions. We prove some properties that are satisfied by the new discrete Funk transform F defined in (1); in particular, we show that the pseudoinverse $\mathrm{F}^\dagger$ represents an *inverse discrete Funk transform* analogous to the direct transform F. And we propose a series of numerical tests which attest to the stability and the accuracy of F.

The paper is organized as follows. In Section 2, we summarize some background concerning spherical harmonics, the Funk transform, and the Cubed Sphere. In Section 3, we present least squares approximation of even functions on the Cubed Sphere, without and with regularization. In Section 4, we introduce and we study the discrete Funk transform F, and the pseudoinverse $\mathrm{F}^\dagger$. In Section 5, the relevance of the approach is shown by various numerical tests, such as test of accuracy on synthetic dMRI signals.

2. Background and notation

2.1. **Spherical harmonics.** We consider spherical coordinates on the sphere $\mathbb{S}^2$, given by

$$x(\theta,\phi) = (\cos\theta\cos\phi, \cos\theta\sin\phi, \sin\theta) \in \mathbb{S}^2, \quad \theta \in [-\tfrac{\pi}{2}, \tfrac{\pi}{2}],\ \phi \in \mathbb{R}.$$

In these coordinates, the real Legendre spherical harmonics of degree $n \geq 0$ are defined by

$$Y_n^m(x(\theta,\phi)) = \sqrt{\tfrac{(n+1/2)(n-|m|)!}{\pi(n+|m|)!}}P_n^{(|m|)}(\sin\theta)\cdot\cos^{|m|}\theta\cdot\begin{cases}-\sin m\phi, & -n \leq m < 0,\\ \frac{1}{\sqrt{2}}, & m = 0,\\ \cos m\phi, & 0 < m \leq n,\end{cases}$$

where $P_n^{(|m|)}(t) = \frac{\mathrm{d}^{|m|}}{\mathrm{d}t^{|m|}}P_n(t)$ is the $|m|$-th derivative of the Legendre polynomial of degree n, defined by

$$P_n(t) = \tfrac{1}{2^n n!}\tfrac{\mathrm{d}^n}{\mathrm{d}t^n}(t^2-1)^n.$$

The infinite family $(Y_n^m)_{|m|\leq n,\, n\in\mathbb{N}}$ is a Hilbert basis of the space $L^2(\mathbb{S}^2)$, which is equiped with the usual inner product and the associated norm,

$$\langle f, g\rangle_{L^2(\mathbb{S}^2)} = \int_{\mathbb{S}^2} f(x)g(x)\mathrm{d}\sigma, \quad \|f\|_{L^2(\mathbb{S}^2)} = \langle f, f\rangle_{L^2(\mathbb{S}^2)}^{1/2}.$$

In this basis, any $f \in L^2(\mathbb{S}^2)$ admits a unique spectral expansion,

$$f = \sum_{|m|\leq n} \hat{f}_n^m Y_n^m, \quad \text{with} \quad \hat{f}_n^m = \langle f, Y_n^m\rangle_{L^2(\mathbb{S}^2)}.$$

For a fixed degree $D \geq 0$, the subspace of the spherical harmonics with degree less than or equal to D is denoted by $\mathcal{Y}_D$, so that $(Y_n^m)_{|m|\leq n\leq D}$ is an orthonormal basis of $\mathcal{Y}_D$. The subspace of even functions in $\mathcal{Y}_D$, denoted by $\mathcal{Y}_D^{\mathrm{ev}}$, is spanned by the even degrees, *i.e.*

$$\mathcal{Y}_D^{\mathrm{ev}} = \mathbb{Y}_0 \oplus \cdots \oplus \mathbb{Y}_{2n} \oplus \cdots \oplus \mathbb{Y}_{2\lfloor D/2\rfloor} = \mathrm{span}\{Y_{2n}^m,\ 0 \leq n \leq \lfloor \tfrac{D}{2}\rfloor,\ |m| \leq 2n\}.$$

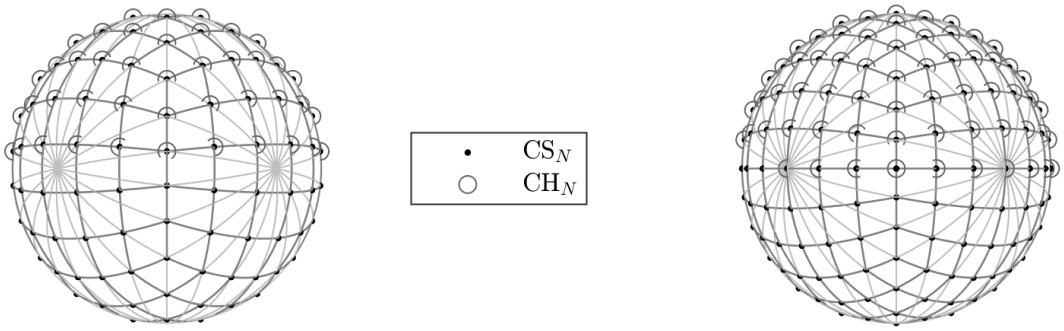

FIGURE 1. Cubed Sphere and Cubed Hemisphere. The Cubed Sphere CS_N (black dots) defined in (4) is obtained by intersecting equiangular meridian circles (gray lines). The Cubed Hemisphere CH_N (gray circles) defined in (6) is located in the Northern hemisphere; it contains half of the points from CS_N. Left: N is odd ($N = 5$). Right: N is even ($N = 6$).

Hence, the dimension of $\mathcal{Y}_D^{\mathrm{ev}}$ is given by

$$d_D = (2\lfloor \tfrac{D}{2} \rfloor + 1)(\lfloor \tfrac{D}{2} \rfloor + 1).$$

2.2. **Funk transform.** The Funk transform, denoted by $\mathcal{F}$, maps a spherical function $f : \mathbb{S}^2 \to \mathbb{R}$ (smooth enough) to a spherical function $\mathcal{F}f : \mathbb{S}^2 \to \mathbb{R}$ as follows. For any unit vector $\alpha \in \mathbb{S}^2$, $\mathcal{F}f(\alpha)$ is the average of f along the great circle that is orthogonal to α, *i.e.*

$$\mathcal{F}f(\alpha) = \frac{1}{2\pi} \int_{\{x \in \mathbb{S}^2 : x \cdot \alpha = 0\}} f \, \mathrm{d}s, \quad \alpha \in \mathbb{S}^2, \quad f : \mathbb{S}^2 \to \mathbb{R},$$

where s denotes the length measure on the circle $\{x \in \mathbb{S}^2 : x \cdot \alpha = 0\}$. The Funk transform $\mathcal{F}f$ is an even function, *i.e.* $\mathcal{F}f(-\alpha) = \mathcal{F}f(\alpha)$, $\alpha \in \mathbb{S}^2$. If f is odd, *i.e.* $f(-x) = -f(x)$, $x \in \mathbb{S}^2$, then $\mathcal{F}f = 0$. In any case, $\mathcal{F}f = \mathcal{F}f^{\mathrm{ev}}$, where $f^{\mathrm{ev}}(x) = \frac{1}{2}(f(x) + f(-x))$ denotes the even part of f. For these reasons, the Funk transform is often considered only between spaces of even functions, without loss of generality. We follow this convention throughout the article.

The Funk transform $\mathcal{F}$ is diagonal in the Legendre basis [14], so that it defines an isomorphism on $\mathcal{Y}_D^{\mathrm{ev}}$,

$$\mathcal{F} : \mathcal{Y}_D^{\mathrm{ev}} \to \mathcal{Y}_D^{\mathrm{ev}}, \quad \mathcal{F}Y_{2n}^m = P_{2n}(0)\, Y_{2n}^m, \quad \text{with} \quad P_{2n}(0) = (-1)^n \tfrac{1 \cdot 3 \cdot 5 \cdots (2n-1)}{2 \cdot 4 \cdot 6 \cdots (2n)}, \\ |m| \le 2n,\ 0 \le n \le \lfloor \tfrac{D}{2} \rfloor. \quad (2)$$

The associated nonsingular matrix is the block diagonal matrix

$$\Lambda_D = \mathrm{diag}\left[(-1)^n \tfrac{1 \cdot 3 \cdot 5 \cdots (2n-1)}{2 \cdot 4 \cdot 6 \cdots (2n)} \mathrm{I}_{4n+1}, 0 \le n \le \lfloor \tfrac{D}{2} \rfloor \right] \in \mathbb{R}^{d_D \times d_D}. \quad (3)$$

This structure suggests the spectral method for the computation of Funk transforms [12].

2.3. **Cubed Sphere.** For a fixed parameter $N \ge 1$, the equiangular Cubed Sphere $\mathrm{CS}_N \subset \mathbb{S}^2$, with angular step $\frac{\pi}{2N}$, is defined analytically by

$$\mathrm{CS}_N := \Big\{ \tfrac{1}{r}(\pm 1, u, v),\ \tfrac{1}{r}(u, \pm 1, v),\ \tfrac{1}{r}(u, v, \pm 1); \\ r = (1 + u^2 + v^2)^{1/2},\ u = \tan(-\tfrac{\pi}{4} + \tfrac{i\pi}{2N}),\ v = \tan(-\tfrac{\pi}{4} + \tfrac{j\pi}{2N}),\ 0 \le i, j \le N \Big\}. \quad (4)$$

From a geometrical point of view, CS_N is obtained by intersecting great circles as in Figure 1. These great circles correspond to $2N$ equiangular meridian circles with polar axis $(0; (0, 0, 1))$, and their counterparts for the axes $(0; (0, 1, 0))$ and $(0; (1, 0, 0))$. The cardinal number of CS_N is given by $6N^2 + 2$. See, for instance, [7].

3. Least squares approximation on the Cubed Hemisphere

We present least squares fitting on the Cubed Sphere, in the spirit of [6]. An original specificity here is that only even functions are considered, which reduces the dimension of the problem.

3.1. **Least squares fitting with central symmetry.** Assume that $b = [b(\xi)]_{\xi\in \mathrm{CS}_N} \in \mathbb{R}^{6N^2+2}$ is a given grid function on the Cubed Sphere CS_N. One looks for an even spherical harmonics $f \in \mathcal{Y}_D^{\mathrm{ev}}$ which fits b. The least squares approximation minimizes a fitting error as follows,

$$\inf_{f\in\mathcal{Y}_D^{\mathrm{ev}}} \sum_{\xi\in\mathrm{CS}_N} (f(\xi)-b(\xi))^2. \tag{5}$$

Without loss of generality, we can assume that b is an even grid function, *i.e.* such that for any $\xi \in \mathrm{CS}_N$, $b(-\xi) = b(\xi)$ with $-\xi \in \mathrm{CS}_N$. Indeed, the Cubed Sphere CS_N is invariant under the central symmetry $-\mathrm{I}_3$ ($x \leftrightarrow -x$) [3], which permits to split b into $b = b^{\mathrm{ev}} + b^{\mathrm{odd}}$, where $b^{\mathrm{ev}}(\xi) = \frac{1}{2}(b(\xi)+b(-\xi))$ is an even grid function, and $b^{\mathrm{odd}}(\xi) = \frac{1}{2}(b(\xi)-b(-\xi))$ is odd ($b^{\mathrm{odd}}(-\xi) = -b^{\mathrm{odd}}(\xi)$). Therefore, for any $f \in \mathcal{Y}_D^{\mathrm{ev}}$,

$$\sum_{\xi\in\mathrm{CS}_N} (f(\xi)-b(\xi))^2 = \sum_{\xi\in\mathrm{CS}_N} (f(\xi)-b^{\mathrm{ev}}(\xi))^2 + \sum_{\xi\in\mathrm{CS}_N} b^{\mathrm{odd}}(\xi)^2 + 2\sum_{\xi\in\mathrm{CS}_N} (f(\xi)-b^{\mathrm{ev}}(\xi))b^{\mathrm{odd}}(\xi).$$

The second term in the right hand side does not depend on f, whereas the third one is null, because $[(f(\xi)-b^{\mathrm{ev}}(\xi))b^{\mathrm{odd}}(\xi)]_{\xi\in\mathrm{CS}_N}$ is an odd grid function. Therefore, the problem (5) is equivalent to

$$\inf_{f\in\mathcal{Y}_D^{\mathrm{ev}}} \sum_{\xi\in\mathrm{CS}_N} (f(\xi)-b^{\mathrm{ev}}(\xi))^2,$$

so that one may assume in (5) that b is even (up to the change $b := b^{\mathrm{ev}}$). This is assumed from now on.

Then, we halve the number of data points based on a splitting of CS_N into two opposite parts. One of the parts, called the *Cubed Hemisphere*, keeps only the Northern hemisphere and a half of the equator circle, as in Figure 1 and in the following definition.

Definition 2. Let $N \geq 1$. The *Cubed Hemisphere* CH_N is defined by

$$\mathrm{CH}_N = \mathrm{CS}_N \cap \{x(\theta,\phi)\in\mathbb{S}^2, \quad (\theta>0 \text{ and } 0\leq\phi<2\pi) \text{ or } (\theta=0 \text{ and } 0\leq\phi<\pi)\}, \tag{6}$$

so that CS_N is the disjoint union $\mathrm{CS}_N = \mathrm{CH}_N \cup (-\mathrm{CH}_N)$, and CH_N has the cardinal number $3N^2+1$.

Clearly, the least squares problem (5) (with an even grid function) is equivalent to

$$\inf_{f\in\mathcal{Y}_D^{\mathrm{ev}}} \sum_{\xi\in\mathrm{CH}_N} (f(\xi)-b(\xi))^2, \tag{LS}$$

where the given grid function is $b = [b(\xi)]_{\xi\in\mathrm{CH}_N} \in \mathbb{R}^{3N^2+1}$. This problem is the main approximation problem in this paper. Introducing the Legendre basis,

$$f = \sum_{0\leq n\leq\lfloor D/2\rfloor, |m|\leq 2n} \hat{f}_n^m Y_{2n}^m \in \mathcal{Y}_D^{\mathrm{ev}}, \quad \text{with} \quad \hat{f} = [f_{2n}^m]_{0\leq n\leq\lfloor D/2\rfloor, |m|\leq 2n} \in \mathbb{R}^{d_D},$$

the matrix of the linear map $f \in \mathcal{Y}_D^{\mathrm{ev}} \mapsto [f(\xi)]_{\xi\in\mathrm{CH}_N} \in \mathbb{R}^{3N^2+1}$ is the Vandermonde matrix

$$A_N^D = [Y_{2n}^m(\xi)]_{\substack{\xi\in\mathrm{CH}_N \\ 0\leq n\leq\lfloor D/2\rfloor, |m|\leq 2n}} \in \mathbb{R}^{(3N^2+1)\times d_D}, \tag{7}$$

so that the problem (LS) can be written in matrix form as

$$\inf_{\hat{f}\in\mathbb{R}^{d_D}} \|A_N^D\hat{f} - b\|^2. \tag{$\widehat{\mathrm{LS}}$}$$

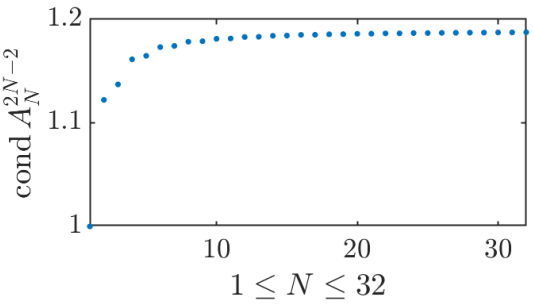

FIGURE 2. Numerical evidence of Claim 3: the condition number of the Vandermonde matrix A_N^D is plotted for $D = 2N - 2$ and $1 \le N \le 32$.

3.2. **Least squares aproximation without regularization.** The well-posedness of the considered problem (LS) depends on the column rank and on the condition number of the matrix A_N^D. We refer to [6], where a similar problem has been studied for the full grid CS_N and the full space $\mathcal{Y}_D$ (without symmetry assumption). In this case, the Vandermonde matrix is given by

$$B_N^D = [Y_n^m(\xi)]_{\substack{\xi\in\mathrm{CS}_N \\ |m|\le n\le D}} \in \mathbb{R}^{(6N^2+2)\times(D+1)^2}. \tag{8}$$

For the degree $D = 2N - 1$, it has been observed in numerical experiments in [6] that B_N^D has full column rank, and has a condition number which is uniformly bounded with N (and close to 1). This property is not valid anymore if $D \ge 2N$, where the critical degree $2N$ corresponds to oscillations at the Nyquist's frequency associated to the angular step $\frac{\pi}{2N}$ of CS_N.

One may expect that similar results apply for the matrix A_N^D, because

$$\begin{bmatrix} A_N^D \\ A_N^D \end{bmatrix}$$

can be extracted from B_N^D (up to a reordering of rows). This motivates the following claim, which is analogous to [6, Claim 2], but deals with even functions only.

Claim 3. *Let $N \ge 1$, and fix the degree $D = 2N - 2$ in (7). Then, the Vandermonde matrix*

$$A_N^{2N-2} = [Y_{2n}^m(\xi)]_{\substack{\xi\in\mathrm{CH}_N \\ 0\le n\le N-1,\, |m|\le 2n}} \in \mathbb{R}^{(3N^2+1)\times(2N-1)N}, \tag{9}$$

has full column rank and is well-conditioned, with a condition number uniformly bounded with N.

We provide a numerical evidence of this claim in Figure 2, where it is observed that

$$\operatorname{cond} A_N^{2N-2} \le 1.2, \quad 1 \le N \le 32.$$

Nevertheless, a theoretical proof of this claim is not available yet (so is the proof of [6, Claim 2]).

Assuming that Claim 3 is true, we set

$$D = 2N - 2, \quad A = A_N^{2N-2}. \tag{10}$$

Then, the problem (LS) admits a unique solution. This solution, denoted by

$$\ell[b] \in \mathcal{Y}_{2N-2}^{\mathrm{ev}}, \quad \ell[b] = \arg \inf_{f\in\mathcal{Y}_{2N-2}^{\mathrm{ev}}} \sum_{\xi\in\mathrm{CH}_N} (f(\xi) - b(\xi))^2, \tag{11}$$

is given by

$$\ell[b] = [Y_{2n}^m(\cdot)]_{0\le n\le N-1,\, |m|\le 2n}^{\intercal}\, \widehat{\ell[b]}, \quad \text{with} \quad \widehat{\ell[b]} = (A^{\intercal}A)^{-1}A^{\intercal}b \in \mathbb{R}^{(2N-1)N}. \tag{12}$$

Here, as a consequence of Claim 3, the vector $\widehat{\ell[b]}$ of the spectral coefficients satisfies a linear system, whose matrix is symmetric, positive-definite, and well-conditioned:

$$A^{\intercal}A\,\widehat{\ell[b]} = A^{\intercal}b.$$

In this case ($D = 2N - 2$), regularization is not needed.

3.3. **Regularized least squares approximation.** For larger values of the degree D, *i.e.* $D \geq 2N$, regularization is advised. This is due to the following result, analogous to [6, Theorem 4].

Proposition 4. *Let $\sigma_{\min}(A_N^D)$, resp. $\mathrm{cond}(A_N^D)$, denote the smallest singular value, resp. condition number, of the Vandermonde matrix A_N^D in (7), $N \geq 1$, $D \geq 0$.*

(i) There exists a sequence $(\epsilon_N)_{N\geq 1}$ with asymptotics behavior

$$\epsilon_N \underset{N\to+\infty}{\sim} \frac{N}{2}\left(\frac{2N}{\pi}\right)^{3/2}\left(\frac{2}{3}\right)^{2N} \underset{N\to+\infty}{\to} 0,$$

such that

$$\forall N \geq 1, \forall D \geq 2N, \quad \sigma_{\min}(A_N^D)^2 \leq \epsilon_N.$$

(ii) There exists a sequence $(M_N)_{N\geq 1}$ with asymptotics behavior

$$M_N \underset{N\to+\infty}{\sim} \frac{1}{4}\left(\frac{\pi}{2N}\right)^{1/2}\left(\frac{3}{2}\right)^{2N+1} \underset{N\to+\infty}{\to} +\infty,$$

such that, for all $N \geq 1$ and $D \geq 2N$ such that A_N^D is injective,

$$\mathrm{cond}(A_N^D)^2 \geq M_N.$$

Proof. We refer to [6, Theorem 4], where the smallest, resp. largest, singular value of B_N^D are dominated considering the examples $f_0 = Y_{2N}^{-2N}(x(\theta, \phi - \frac{\pi}{4})) \in \mathcal{Y}_{2N}$, resp. $f_1 = Y_0 \in \mathcal{Y}_{2N}$. The same strategy applies for A_N^D, since f_0, $f_1 \in \mathcal{Y}_{2N}^{\mathrm{ev}}$. So we get almost the same estimations; the slight difference is a factor $\frac{1}{2}$, due to the restriction of CS_N to CH_N. This factor disappears in the estimation of the condition number since it is a ratio. □

As a consequence of this proposition, the least squares problem (LS) is ill-posed if N is "large" and $D \geq 2N$: in this case, the matrix A_N^D of the problem has a large condition number, or is not injective. That is the reason why regularization is at least advised (or even needed) if $D \geq 2N$. We refer to [16] for a general reference about ill-posed problems, including Tikhonov regularization, and we refer to [1] for various regularization operators dealing with spherical harmonics on the sphere.

In this paper, we consider a Tikhonov regularization of (LS), in the spirit of [12]. We add a weighted penalty in the misfit function based on the Laplace-Beltrami operator: we introduce the least squares problem

$$\inf_{f\in\mathcal{Y}_D^{\mathrm{ev}}} \sum_{\xi\in\mathrm{CH}_N} (f(\xi) - b(\xi))^2 + \lambda \|\Delta_{\mathrm{S}} f\|^2_{L^2(\mathbb{S}^2)}, \tag{RLS}$$

where $\lambda \geq 0$ is a fixed weight, and Δ_{S} is the Laplace-Beltrami operator. It is classical (see [2] for instance) that Δ_{S} is diagonal in the Legendre basis, with

$$\Delta_{\mathrm{S}} Y_n^m = -n(n+1)Y_n^m, \quad 0 \leq |m| \leq n.$$

So, the regularized problem (RLS) is expressed in matrix form as

$$\inf_{\hat{f}\in\mathbb{R}^{d_D}} \|A_N^D \hat{f} - b\|^2 + \lambda \|\Delta_D \hat{f}\|^2, \tag{$\widehat{\mathrm{RLS}}$}$$

where Δ_D is the block diagonal matrix

$$\Delta_D = \mathrm{diag}\left[-n(n+1)\,\mathrm{I}_{4n+1}, 0 \leq n \leq \lfloor \tfrac{D}{2} \rfloor\right] \in \mathbb{R}^{d_D \times d_D}. \tag{13}$$

The following lemma shows that the proposed regularization guarantees existence and uniqueness of an approximating function.

Lemma 5. *Assume that $\lambda > 0$, or that A_N^D has full column rank. Then, the regularized problem* (RLS)*, and* ($\widehat{\mathrm{RLS}}$)*, have a unique solution, given by*

$$\ell_\lambda[b] = [Y_{2n}^m(\cdot)]_{0\leq n\leq \lfloor D/2\rfloor, |m|\leq 2n}^{\intercal} \widehat{\ell_\lambda[b]}, \text{ with } \widehat{\ell_\lambda[b]} = \left[(A_N^D)^{\intercal} A_N^D + \lambda \Delta_D^2\right]^{-1} (A_N^D)^{\intercal} b \in \mathbb{R}^{d_D}, \tag{14}$$

where the matrix

$$(A_N^D)^{\intercal} A_N^D + \lambda \Delta_D^2 \tag{15}$$

is symmetric and positive definite.

Proof. It is not difficult to check that

$$\mathrm{Ker}(A_N^D) \cap \mathrm{Ker}(\lambda^{1/2}\Delta_D) = \{0\},$$

which implies the result, as in [16, Chapter 5]. □

Introducing the regularized problem (RLS) is interesting from a theoretical point of view, since it permits to guarantee existence and uniqueness of a fitting function on CH_N, for any approximation space $\mathcal{Y}_D^{\mathrm{ev}}$, $D \geq 0$. Nevertheless, in practice, the degree D must be selected, and the weight $\lambda \geq 0$ must be tuned to adjust the balance between the regularizing term and the fitting error. For the purpose of this paper, we emphasize in Section 5 that the value $\lambda = 0$ gives very satisfactory results for the degree $D = 2N-2$; in this case, $\ell_0[b] = \ell[b]$ in (12) and there is no regularization. In other words, it is not really worth regularizing in practice; the grid CH_N and the approximation space $\mathcal{Y}_{2N-2}^{\mathrm{ev}}$ are competitive for approximating the Funk transform.

4. Discrete Funk transform and its pseudoinverse

We introduce and we study a new discrete Funk transform, dedicated to the Cubed Sphere.

4.1. **Motivation of Definition 1.** First, we recall a spectral method for approximating the Funk transform. It is based on least squares approximation in a space of spherical harmonics, with Laplace-Beltrami regularization. This popular approach has been introduced in [12], for a general grid. Here, we assume that we know a grid function $b = [b(\xi)]_{\xi \in \mathrm{CH}_N} \in \mathbb{R}^{3N^2+1}$ on the Cubed Hemisphere CH_N. As in Subsection 3.1, b has eventually been computed as the restriction to CH_N of the even part of a grid function known on CS_N. Then, we compute the Funk transform of a spherical function which fits the data b on CH_N. More precisely, we introduce a least squares approximation of b in $\mathcal{Y}_D^{\mathrm{ev}}$. According to Lemma 5, we can introduce the solution $\ell_\lambda[b] \in \mathcal{Y}_D^{\mathrm{ev}}$ to a regularized problem (RLS). In this case, we can compute the Funk transform $\mathcal{F}[\ell_\lambda[b]]$, where $\ell_\lambda[b]$ is defined in (14); using the spectral form of $\mathcal{F}$, this is expressed in exact analytical form as

$$\mathcal{F}[\ell_\lambda[b]](\alpha) = [Y_{2n}^m(\alpha)]_{0\leq n\leq \lfloor D/2\rfloor,\, |m|\leq 2n}^{\intercal} \Lambda_D \left[(A_N^D)^{\intercal} A_N^D + \lambda \Delta_D^2\right]^{-1} (A_N^D)^{\intercal} b, \quad \alpha \in \mathbb{S}^2, \tag{16}$$

where Λ_D is the diagonal matrix associated to $\mathcal{F} : \mathcal{Y}_D^{\mathrm{ev}} \to \mathcal{Y}_D^{\mathrm{ev}}$, defined in (13). In this way, we map a vector $b \in \mathbb{R}^{3N^2+1}$ of values on CH_N towards the spherical harmonics $\mathcal{F}[\ell_\lambda[b]] \in \mathcal{Y}_D^{\mathrm{ev}}$. If $f : \mathbb{S}^2 \to \mathbb{R}$ is an even spherical function, we can set $b = [f(\xi)]_{\xi \in \mathrm{CH}_N}$, so that $\ell_\lambda[b]$ is expected to approximate f on $\mathbb{S}^2$, and $\mathcal{F}[\ell_\lambda[b]]$ is expected to approximate $\mathcal{F}f$. In other words, (16) is expected to estimate the integral of f along any great circle $x \cdot \alpha = 0$, from the grid values $b = [f(\xi)]_{\xi \in \mathrm{CH}_N}$ only.

The new feature in our work is that the considered grid is the Cubed Hemisphere CH_N (or the Cubed Sphere CS_N itself). Therefore, the result from Claim 3 is expected. As in Subsection 3.2, this suggests to set $D = 2N-2$ and to solve the original least squares problem (LS) without regularization ($\lambda = 0$). Then, computing the Funk transform of this approximation leads to a new spectral method, which computes a Funk transform in $\mathcal{Y}_{2N-2}^{\mathrm{ev}}$ from grid values $b = [b(\xi)]_{\xi \in \mathrm{CH}_N} \in \mathbb{R}^{3N^2+1}$,

$$\mathcal{F}[\ell[b]](\alpha) = [Y_{2n}^m(\alpha)]_{0\leq n\leq N-1,\, |m|\leq 2n}^{\intercal} \Lambda \left(A^{\intercal} A\right)^{-1} A^{\intercal}\, b, \quad \alpha \in \mathbb{S}^2, \tag{17}$$

where $A = A_N^{2N-2}$ in (9), $\Lambda = \Lambda_{2N-2}$, and $\ell[b]$ is the approximation defined in (12).

The last step to obtain our discrete Funk transform on CH_N is to sample the spherical function $\mathcal{F}[\ell[b]]$ on CH_N. In other words, we define the discrete Funk transform of the grid function $b = [b(\xi)]_{\xi \in \mathrm{CH}_N}$ as the grid function $[\mathcal{F}[\ell[b]](\alpha)]_{\alpha \in \mathrm{CH}_N}$, where ξ is the original spatial variable on $\mathbb{S}^2$, and the "dual" variable α represents the normal vectors to the great circles. In this way, we obtain exactly

$$[\mathcal{F}[\ell[b]](\alpha)]_{\alpha \in \mathrm{CH}_N} = \mathrm{F}\, b,$$

where the matrix F is defined in (1), and is the so-called *discrete Funk transform* in Definition 1.

Lastly, we comment the full column rank condition that is formulated in Definition 1. This condition has been included in the text of the definition to guarantee that F in (1) is defined.

We do not have a proof that this condition is satisfied for any $N \geq 1$, but Claim 3 indicates that it is expected, with a nice condition number for $A^\intercal A$.

4.2. **Properties of the discrete Funk transform.** In this subsection, we keep the notation from Definition 1; we assume that $N \geq 1$ is such that $A = A_N^{2N-2}$ has full column rank, so that the discrete Funk transform F is defined. We prove of series of properties satisfied by this new transform.

The discrete Funk transform F has been defined to satisfy the following property.

Property 6. *For any $b = [b(\xi)]_{\xi \in \mathrm{CH}_N} \in \mathbb{R}^{3N^2+1}$, the discrete Funk transform $\mathrm{F}b \in \mathbb{R}^{3N^2+1}$ is the restriction to CH_N of the Funk transform of the least squares fitting $\ell[b] \in \mathcal{Y}_{2N-2}^{\mathrm{ev}}$,*

$$\mathrm{F}b = [\mathcal{F}[\ell[b]](\alpha)]_{\alpha \in \mathrm{CH}_N}, \quad \ell[b] = \arg \inf_{f \in \mathcal{Y}_{2N-2}^{\mathrm{ev}}} \sum_{\xi \in \mathrm{CH}_N} (f(\xi) - b(\xi))^2. \tag{18}$$

Proof. Since A has full column rank, there exists a unique solution $\ell[b]$ to (LS), and it is given by (12). Then, the Funk transform is a multiplication of the spectral coefficients by Λ, so that $\mathcal{F}[\ell[b]]$ is given by (17). Finally, the evaluation on CH_N is a multiplication of the spectral coefficients by the Vandermonde matrix A, so that $\mathrm{F}b$ coincides with $[\mathcal{F}[\ell[b]](\alpha)]_{\alpha \in \mathrm{CH}_N}$. □

The discrete transform $\mathrm{F}b$ is the restriction to CH_N of the spherical function $\mathcal{F}[\ell[b]]$; the following result establishes that this restriction is lossly, since $\mathcal{F}[\ell[b]]$ can be recovered from $\mathrm{F}b$ by least squares fitting. In other words, the transform F is "equivalent" to $\mathcal{F}[\ell[\cdot]]$.

Proposition 7. *The least squares fitting $\ell[\mathrm{F}b]$ of the discrete Funk transform $\mathrm{F}b$ coincides with the Funk transform of the least squares fitting $\ell[b]$ of b,* i.e.

$$\ell[\mathrm{F}b](\alpha) = \mathcal{F}[\ell[b]](\alpha), \quad b \in \mathbb{R}^{3N^2+1}, \, \alpha \in \mathbb{S}^2. \tag{19}$$

Proof. The spectral coefficients of $\ell[\mathrm{F}b] \in \mathcal{Y}_{2N-2}^{\mathrm{ev}}$ are given by (12) and (1),

$$\begin{aligned} \widehat{\ell[\mathrm{F}b]} &= (A^\intercal A)^{-1} A^\intercal \, \mathrm{F}b \\ &= (A^\intercal A)^{-1} A^\intercal A \, \Lambda \, (A^\intercal A)^{-1} A^\intercal \, b \\ &= \Lambda \, (A^\intercal A)^{-1} A^\intercal \, b, \end{aligned}$$

so they coincide with the spectral coefficients of $\mathcal{F}[\ell[b]] \in \mathcal{Y}_{2N-2}^{\mathrm{ev}}$, given in (17). □

In practice, if $f : \mathbb{S}^2 \to \mathbb{R}$ is spherical a function, one can use the discrete Funk transform $\mathrm{F}[f(\xi)]_{\xi \in \mathrm{CH}_N}$, or equivalently $\mathcal{F}[\ell[f(\xi)]_{\xi \in \mathrm{CH}_N}]$, in order to approximate some values $\mathcal{F}f(\alpha)$ of the Funk transform $\mathcal{F}f$. The following result shows that this method is exact if $f \in \mathcal{Y}_{2N-2}^{\mathrm{ev}}$.

Theorem 8 (Exactness on $\mathcal{Y}_{2N-2}^{\mathrm{ev}}$)**.** *For every $f \in \mathcal{Y}_{2N-2}^{\mathrm{ev}}$, the Funk transform $\mathcal{F}[f]$ can be computed exactly from the grid values $[f(\xi)]_{\xi \in \mathrm{CH}_N}$,*

$$\begin{aligned} \mathcal{F}[f](\alpha) &= \mathcal{F}[\ell[f(\xi)]_{\xi \in \mathrm{CH}_N}](\alpha), \\ &= [Y_{2n}^m(\alpha)]_{0 \leq n \leq N-1, \, |m| \leq 2n}^\intercal \Lambda \, (A^\intercal A)^{-1} \, A^\intercal \, [f(\xi)]_{\xi \in \mathrm{CH}_N}, \quad \alpha \in \mathbb{S}^2, \quad f \in \mathcal{Y}_{2N-2}^{\mathrm{ev}}. \end{aligned} \tag{20}$$

In particular, on the grid CH_N,

$$[\mathcal{F}[f](\alpha)]_{\alpha \in \mathrm{CH}_N} = \mathrm{F}[f(\xi)]_{\xi \in \mathrm{CH}_N}, \quad f \in \mathcal{Y}_{2N-2}^{\mathrm{ev}}. \tag{21}$$

Proof. Any function $f \in \mathcal{Y}_{2N-2}^{\mathrm{ev}}$ fits exactly the grid values $[f(\xi)]_{\xi \in \mathrm{CH}_N}$, so that the unique solution of (LS) with $b = [f(\xi)]$ is the initial function f itself,

$$\ell[f(\xi)]_{\xi \in \mathrm{CH}_N} = f, \quad f \in \mathcal{Y}_{2N-2}^{\mathrm{ev}}.$$

Injecting this equality into (17) and (18) proves the desired results. □

Now, we investigate the inversion of the Funk transform F. We do not expect the discrete transform F to be nonsingular. Therefore, we introduce the Moore-Penrose pseudoinverse $\mathrm{F}^\dagger$ (instead of an inverse). We refer to [15, pp. 257-258] for usual consideration about the Moore-Penrose pseudoinverse. In our case, the pseudoinverse $\mathrm{F}^\dagger$ maps any $c \in \mathbb{R}^{3N^2+1}$ to the minimum norm solution $b = \mathrm{F}^\dagger c \in \mathbb{R}^{3N^2+1}$ of the least squares problem $\inf_{b \in \mathbb{R}^{3N^2+1}} \|\mathrm{F}b - c\|^2$.

Here, we prove that the Moore-Penrose pseudoinverse $\mathrm{F}^\dagger$ of F represents an *inverse discrete Funk transform* that is very analogous to the direct transform F.

Theorem 9 (Pseudoinversion). *The Moore-Penrose pseudoinverse of* F *is given by*

$$\mathrm{F}^\dagger = A\,\Lambda^{-1}\,(A^\intercal A)^{-1}A^\intercal \in \mathbb{R}^{(3N^2+1)\times(3N^2+1)}. \tag{22}$$

Therefore, for any $c = [c(\alpha)]_{\alpha\in\mathrm{CH}_N} \in \mathbb{R}^{3N^2+1}$, *the pseudoinverse* $\mathrm{F}^\dagger c \in \mathbb{R}^{3N^2+1}$ *represents the inverse Funk transform of the least squares fitting* $\ell[c] \in \mathcal{Y}^{\mathrm{ev}}_{2N-2}$, *restricted to* CH_N,

$$\mathrm{F}^\dagger c = \big[\mathcal{F}^{-1}[\ell[c]](\xi)\big]_{\xi\in\mathrm{CH}_N}, \quad \ell[c] = \arg\inf_{f\in\mathcal{Y}^{\mathrm{ev}}_{2N-2}} \sum_{\alpha\in\mathrm{CH}_N} (f(\alpha)-c(\alpha))^2. \tag{23}$$

Hence, the pseudoinverse $\mathrm{F}^\dagger$ *is also called the* inverse discrete Funk transform on CH_N.

Proof. The matrix $\mathrm{F}^\dagger$ is the Moore-Penrose pseudoinverse of F (and conversely), because (1) and (22) imply that the four Moore-Penrose conditions [15, p. 257] are satisfied:

$$\mathrm{F}\mathrm{F}^\dagger\mathrm{F} = \mathrm{F}, \quad \mathrm{F}^\dagger\mathrm{F}\mathrm{F}^\dagger = \mathrm{F}^\dagger, \quad (\mathrm{F}\mathrm{F}^\dagger)^\intercal = \mathrm{F}\mathrm{F}^\dagger, \quad (\mathrm{F}^\dagger\mathrm{F})^\intercal = \mathrm{F}^\dagger\mathrm{F}.$$

The property (23) is derived analogously to (18); the only difference is that the diagonal matrix Λ of the isomorphic Funk transform $\mathcal{F} : \mathcal{Y}^{\mathrm{ev}}_{2N-2} \to \mathcal{Y}^{\mathrm{ev}}_{2N-2}$ is replaced by the inverse diagonal matrix Λ^{-1}, which corresponds to the inverse transform $\mathcal{F}^{-1}$. □

The relations (1) and (22) are very similar, so are (18) and (23). More generally, as soon as some result is established for one of the transforms F and $\mathrm{F}^\dagger$, some counterpart is expected for the other one. For instance, the counterpart of Proposition 7 is given hereafter.

Proposition 10. *The least squares fitting* $\ell[\mathrm{F}^\dagger c]$ *of the inverse discrete Funk transform* $\mathrm{F}^\dagger c$ *coincides with the inverse Funk transform of the least squares fitting* $\ell[c]$ *of* c, i.e.

$$\ell[\mathrm{F}^\dagger c](\xi) = \mathcal{F}^{-1}[\ell[c]](\xi), \quad c \in \mathbb{R}^{3N^2+1},\ \xi \in \mathbb{S}^2.$$

Proof. Analogous to the proof of Proposition 7. □

Now, we express mapping properties of F and $\mathrm{F}^\dagger$ in term of $\operatorname{Ran} A$. In particular, we prove that the transform $\mathrm{F}^\dagger$ is the usual inverse transform of F, if the spaces are restricted to $\operatorname{Ran} A$.

Proposition 11. *The following assertions hold.*

(i) The composition of F *and* $\mathrm{F}^\dagger$ *coincides with the orthogonal projection on* $\operatorname{Ran} A$, *and represents the evaluation on* CH_N *of the least squares approximation* $\ell[\cdot] \in \mathcal{Y}^{\mathrm{ev}}_{2N-2}$,

$$\mathrm{F}\mathrm{F}^\dagger = \mathrm{F}^\dagger\mathrm{F} = A(A^\intercal A)^{-1}A^\intercal = [\ell[\cdot](\xi)]_{\xi\in\mathrm{CH}_N}. \tag{24}$$

In particular,

$$\forall b \in \operatorname{Ran} A, \quad \mathrm{F}^\dagger\mathrm{F}\,b = \mathrm{F}\mathrm{F}^\dagger\,b = b. \tag{25}$$

(ii) The null space and the range of F *satisfy*

$$\operatorname{Ker}\mathrm{F} = \operatorname{Ker} A^\intercal = (\operatorname{Ran} A)^\perp, \quad \operatorname{Ran}\mathrm{F} = \operatorname{Ran} A, \quad \mathbb{R}^{3N^2+1} = \operatorname{Ker}\mathrm{F} \overset{\perp}{\oplus} \operatorname{Ran}\mathrm{F}.$$

(iii) The null space and the range of $\mathrm{F}^\dagger$ *satisfy* $\operatorname{Ker}\mathrm{F}^\dagger = \operatorname{Ker}\mathrm{F}$, $\operatorname{Ran}\mathrm{F}^\dagger = \operatorname{Ran}\mathrm{F}$.

(iv) Restricting the discrete transforms F *and* $\mathrm{F}^\dagger$ *to* $\operatorname{Ran} A$ *defines two isomorphisms*

$$\mathrm{F}|_{\operatorname{Ran} A} : b \in \operatorname{Ran} A \mapsto \mathrm{F}b \in \operatorname{Ran} A, \quad \mathrm{F}^\dagger|_{\operatorname{Ran} A} : c \in \operatorname{Ran} A \mapsto \mathrm{F}^\dagger c \in \operatorname{Ran} A,$$

where $\mathrm{F}^\dagger|_{\operatorname{Ran} A}$ *is the inverse of* $\mathrm{F}|_{\operatorname{Ran} A}$.

Proof. (i) Since A has full column rank, the orthogonal projection on $\operatorname{Ran} A$ is given by the matrix $\Pi = A(A^\intercal A)^{-1}A^\intercal$. This matrix represents the evaluation on CH_N of the least squares approximation, *i.e.* $\Pi b = [\ell[b](\xi)]_{\xi\in\mathrm{CH}_N}$, with $\ell[b]$ in (12). Then $\mathrm{F}\mathrm{F}^\dagger = \mathrm{F}^\dagger\mathrm{F} = \Pi$ can be easily checked with (1) and (22). And this implies (25) due to $\Pi b = b$, for any $b \in \operatorname{Ran} A$.
(ii) The orthogonal decomposition $\mathbb{R}^{3N^2+1} = \operatorname{Ker} A^\intercal \oplus \operatorname{Ran} A$ is a consequence of classical linear algebra. Secondly, $\operatorname{Ker} A^\intercal \subset \operatorname{Ker}\mathrm{F}$ is easily seen in (1), while, $\operatorname{Ker}\mathrm{F} \subset \operatorname{Ker}\mathrm{F}^\dagger\mathrm{F} = \operatorname{Ker}\Pi$, with $\operatorname{Ker}\Pi = (\operatorname{Ran} A)^\perp$. Thirdly, $\operatorname{Ran} F \subset \operatorname{Ran} A$ is easily seen in (1); furthermore, (25) proves that

$\operatorname{Ran} A \subset \operatorname{Ran} \mathrm{F}\mathrm{F}^\dagger$, while $\operatorname{Ran} \mathrm{F}\mathrm{F}^\dagger \subset \operatorname{Ran} \mathrm{F}$.
(iii) The null space and the range of $\mathrm{F}^\dagger$ are obtained analogously as those of F.
(iv) is an obvious consequence of (ii), (iii) and (25). □

To finish with, we provide estimations of stability in term of $\operatorname{cond} A$. They show that stability is expected.

Theorem 12 (Stability). *Let $\sigma_{\max}(\mathrm{F})$ and $\sigma_{\max}(\mathrm{F}^\dagger)$ denote the maximum singular value of* F *and* $\mathrm{F}^\dagger$*,*

$$\sigma_{\max}(\mathrm{F}) = \sup_{\|b\|=1} \|\mathrm{F}b\|, \quad \sigma_{\max}(\mathrm{F}^\dagger) = \sup_{\|c\|=1} \|\mathrm{F}^\dagger c\|. \tag{26}$$

Then,

$$\sigma_{\max}(\mathrm{F}) \leq \operatorname{cond} A, \quad \sigma_{\max}(\mathrm{F}^\dagger) \leq \frac{\operatorname{cond} A}{|P_{2N-2}(0)|} \underset{N\to\infty}{\sim} \sqrt{\pi N} \operatorname{cond} A, \tag{27}$$

where $\operatorname{cond} A$ *is expected to be uniformly bounded due to Claim 3.*

Remark 13. The largest singular values represent stability constants, since perturbing a grid function $b \in \mathbb{R}^{3N^2+1}$ by $\epsilon \in \mathbb{R}^{3N^2+1}$ induces a perturbation on the transform $\mathrm{F}b$, resp. $\mathrm{F}^\dagger b$, which satisfies $\|\mathrm{F}(b+\epsilon) - \mathrm{F}b\| \leq \sigma_{\max}(\mathrm{F})\|\epsilon\|$, $\|\mathrm{F}^\dagger(b+\epsilon) - \mathrm{F}^\dagger b\| \leq \sigma_{\max}(\mathrm{F}^\dagger)\|\epsilon\|$.

Proof. Fix $b \in \mathbb{R}^{3N^2+1}$. We deduce from (1) that

$$\|\mathrm{F}b\| \leq \sigma_{\max}(A)\, \|\Lambda A^\dagger\, b\|,$$

where $\sigma_{\max}(A)$ denotes the maximum singular value of A, and $A^\dagger = (A^\intercal A)^{-1} A^\intercal$ is the Moore-Penrose pseudoinverse of the injective matrix A. Therefore,

$$\|\mathrm{F}b\| \leq \sigma_{\max}(A)\, \sigma_{\max}(\Lambda) \|A^\dagger\, b\| \leq \sigma_{\max}(A)\, \sigma_{\max}(\Lambda)\, \sigma_{\max}(A^\dagger)\, \|b\|.$$

Here, $\sigma_{\max}(\Lambda)$ denotes the maximum singular value of the Funk matrix Λ in (3), and $\sigma_{\max}(A^\dagger)$ denotes the maximum singular value of the pseudoinverse $A^\dagger$. These two values are given by $\sigma_{\max}(\Lambda) = P_0(0) = 1$, and $\sigma_{\max}(A^\dagger) = \frac{1}{\sigma_{\min}(A)}$, where $\sigma_{\min}(A)$ denotes the minimum singular value of A. Finally, we obtain

$$\|\mathrm{F}b\| \leq \frac{\sigma_{\max}(A)}{\sigma_{\min}(A)} \|b\| = \operatorname{cond}(A)\, \|b\|, \quad b \in \mathbb{R}^{3N^2+1},$$

which proves that $\sigma_{\max}(\mathrm{F}) \leq \operatorname{cond}(A)$. For the pseudoinverse $\mathrm{F}^\dagger$ in (22), a very similar computation shows that

$$\|\mathrm{F}^\dagger c\| \leq \sigma_{\max}(A)\, \sigma_{\max}(\Lambda^{-1})\, \sigma_{\max}(A^\dagger)\, \|c\| = \frac{\operatorname{cond}(A)}{|P_{2N-2}(0)|} \|c\|, \quad c \in \mathbb{R}^{3N^2+1},$$

where $\sigma_{\max}(\Lambda^{-1}) = \frac{1}{|P_{2N-2}(0)|}$ is the maximum singular value of Λ^{-1}, with $P_{2N-2}(0)$ given by (2). Therefore, $\sigma_{\max}(\mathrm{F}^\dagger) \leq \frac{\operatorname{cond} A}{|P_{2N-2}(0)|}$. Lastly, the asymptotics $\frac{1}{|P_{2N-2}(0)|} \sim \sqrt{\pi N}$ can checked with the Stirling formula $n! \sim \sqrt{2\pi n} \exp(-n) n^n$. □

5. Numerical results

5.1. **Accuracy of the discrete Funk transform.** We evaluate the accuracy of the discrete Funk transform when it is used to approximate Funk transforms from values on CH_N.

For that purpose, we introduce test functions,

$$g^{(k)} := \sum_{\substack{0\leq n\leq 100 \\ n\equiv 0\,(2)}} \sum_{-n\leq m\leq n} \hat{g}_n^{(k)} (2 + 0.5\cos(m) + 0.25\sin(m))\, Y_n^m \in \mathcal{Y}_{100}^{\mathrm{ev}}, \tag{28}$$

$$\hat{g}_n^{(-\infty)} := \tfrac{1}{n!}, \quad \hat{g}_n^{(k)} := (n+1)^k,\ k = -6, -4, -2, -1, 0, \tag{29}$$

where the various rates of decay of the spectral coefficients encode various "smoothness" properties. Here, $g^{(k)} \in \mathcal{Y}_{100}^{\mathrm{ev}}$, so the values $\mathcal{F}g^{(k)}(\alpha)$ can be exactly computed with (20) from the grid values $[g^{(k)}(\xi)]_{\xi\in\mathrm{CH}_{51}}$.

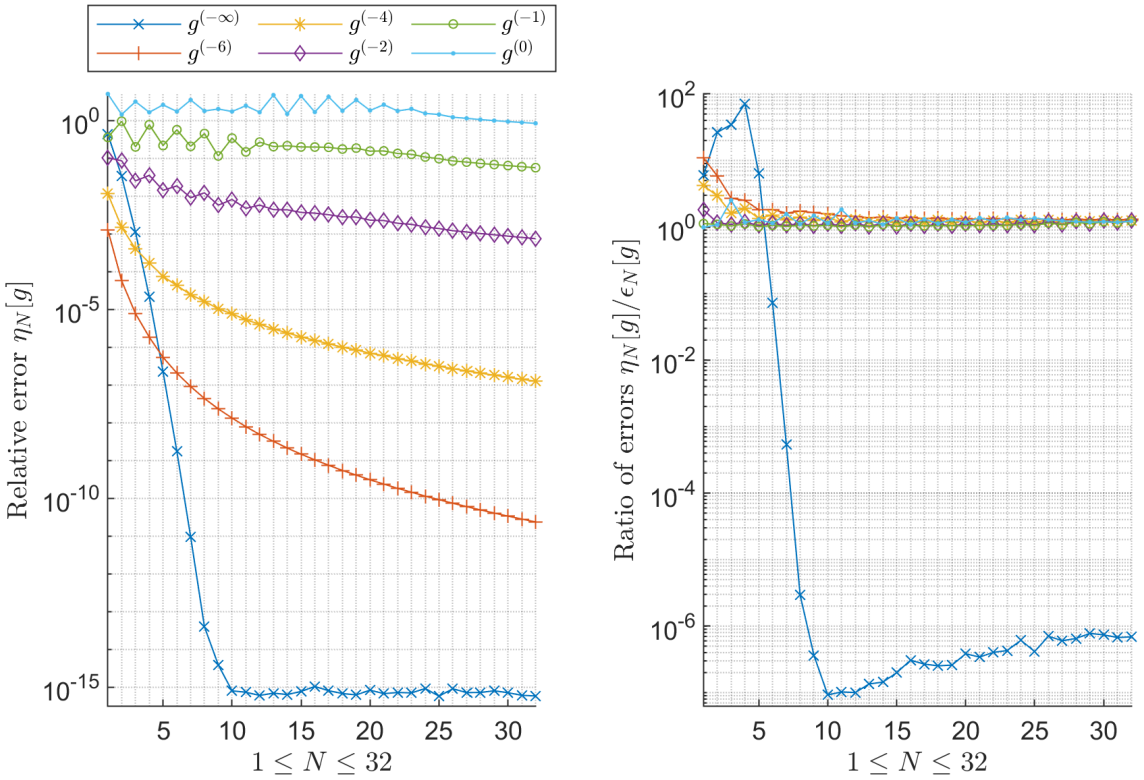

FIGURE 3. Approximation of the Funk transform $[\mathcal{F}g(\alpha)]_{\alpha\in \mathrm{CH}_N}$ by discrete transforms, for the test functions $g = g^{(k)}$ from (28-29). Left: we plot the relative errors $\eta_N[g]$ in (30), associated to the approximation by $\mathrm{F}[g(\xi)]_{\xi\in\mathrm{CH}_N}$. Right: the ratios $\eta_N[g^{(k)}]/\epsilon_N[g^{(k)}]$ are plotted, where $\epsilon_N[g]$ in (35) represents the best relative error among the approximations $\mathrm{F}_{\lambda,D}[g(\xi)]_{\xi\in\mathrm{CH}_N}$ in (33), with D in (32), and λ in (34).

More generally, on the grid CH_N, the Funk transform $\mathcal{F}g^{(k)}$ is approximated by the discrete Funk transform $\mathrm{F}[g^{(k)}(\xi)]$ with a relative error $\eta_N[g^{(k)}]$, where

$$\eta_N[g] := \left(\frac{\sum_{\alpha\in\mathrm{CH}_N} \left[\mathrm{F}[g(\xi)]_{\xi\in\mathrm{CH}_N}(\alpha) - \mathcal{F}g(\alpha)\right]^2}{\sum_{\alpha\in\mathrm{CH}_N} \left[\mathcal{F}g(\alpha)\right]^2} \right)^{1/2}. \tag{30}$$

We have plotted these errors in Figure 3 (left panel), for $1 \leq N \leq 32$. Overall, the behavior of the observed error depends on the rate of decay of the spectral coefficients; the error converges fastly to zero for rapidly decaying coefficients.

We quantify this phenomenon in Table 1, where we report numerical convergence rates $r_N[g]$ such that

$$\eta_{2N}[g] = \eta_N[g]\, 2^{-r_N[g]}, \quad \text{with} \quad r_N[g] = \log_2 \eta_N[g] - \log_2 \eta_{2N}[g]. \tag{31}$$

For $g^{(-\infty)}$, with a factorial decay of the coefficients, $\hat{g}_n^{(-\infty)} = 1/n!$, the very fast convergence appears as a blow up of the rate $r_N[g^{(-\infty)}]$. For the functions $g^{(-k)}$, $k = 6, 4, 2$, with a decay $\hat{g}_n^{(-k)} = 1/(n+1)^k$, the rate looks like $r_N[g^{(-k)}] \approx k - 0.5$. For $g^{(-1)}$, with the slow decay $\hat{g}_n^{(-1)} = 1/(n+1)$, and $g^{(0)}$ with constant values $\hat{g}_n^{(0)} = 1$, the convergence analysis is not so clear.

In a word, the discrete Funk transform F permits to approximate Funk transforms. It converges fastly for smooth functions, for which the spectral coefficients decay rapidly to zero. The observed rates of convergence suggests to analyze theoretically the speed of convergence in Sobolev spaces. We defer this point to further studies.

N	$r_N[g^{(-\infty)}]$	$r_N[g^{(-6)}]$	$r_N[g^{(-4)}]$	$r_N[g^{(-2)}]$	$r_N[g^{(-1)}]$	$r_N[g^{(0)}]$
1	3.7	4.5	2.9	0.28	-1.4	1.8
2	11	4.9	3.1	1.3	0.3	-0.19
4	29	5.4	3.4	1.5	0.78	-0.11
8	5.3	5.4	3.4	1.8	1.2	0.093
16	0.83	5.5	3.6	2.2	1.8	1

TABLE 1. Convergence rates (31) of the errors (30).

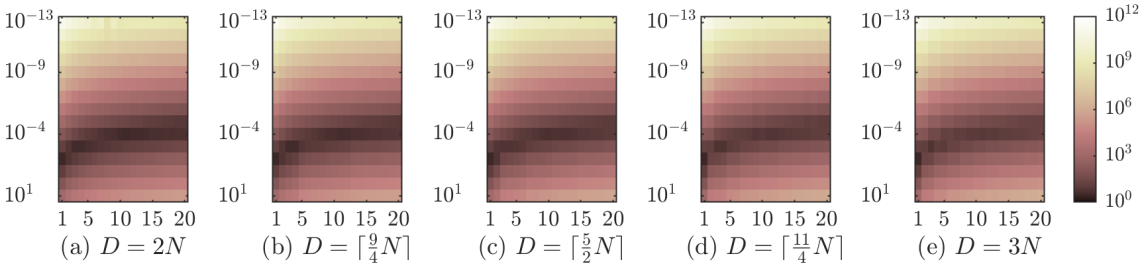

(a) $D = 2N$ (b) $D = \lceil \frac{9}{4}N \rceil$ (c) $D = \lceil \frac{5}{2}N \rceil$ (d) $D = \lceil \frac{11}{4}N \rceil$ (e) $D = 3N$

FIGURE 4. Condition number of the matrix (15), for regularized least squares approximation (14) in $\mathcal{Y}_D^{\mathrm{ev}}$, on the grid CH_N. Five rules are chosen for the degree D (from left to right). The abscissa is the parameter of the grid, $1 \leq N \leq 20$. The ordinate is the regularization parameter $10^{-13} \leq \lambda \leq 10^{1}$ (logarithmic scale). The color represents the condition number (logarithmic scale).

5.2. **Comparison with regularized least squares problems.** We compare our discrete Funk transform F with the transform from (16), where regularized least squares are considered.

Firstly, we consider the conditioning of the least squares problem. For the transform F, based on (LS) with $D = 2N - 2$, the condition number is closed to 1, as already observed in Figure 2. For the transform $\mathcal{F}[\ell_\lambda[\cdot]]$ in (16), associated to the regularization (RLS), we compute the condition number of the matrix from (15). We select various values of the parameters D, λ, with $1 \leq N \leq 20$. The regularization parameter λ is fixed to 10^p, with $-13 \leq p \leq 1$. The degree D browses five values between $2N$ and $3N$,

$$D = 2N,\ 2N + \lceil \tfrac{N}{4} \rceil,\ 2N + \lceil \tfrac{N}{2} \rceil,\ 2N + \lceil \tfrac{3N}{4} \rceil,\ 3N. \tag{32}$$

The lowest value $D = 2N$ is the smallest degree for which regularization is strongly advised according to Claim 3 and Proposition 4; the highest value $D = 3N$ guarantees in practice the existence of an interpolating function in $\mathcal{Y}_D$ when the grid is CS_N [4]. The computed condition numbers are displayed in Figure 4. Some pattern in (N, λ) is observed; it is similar for the five selected rules on the degree D. The results indicate that for (RLS) with $D \geq 2N$, the weight λ must be carefully chosen to obtain a reasonable condition number; $\lambda \approx 10^{-3}$, 10^{-4} is advised.

Secondly, we compare the accuracy of the discrete Funk transform F with similar transforms based on (16). For any test function $g = g^{(k)}$ in (28-29), we approximate $[\mathcal{F}g(\alpha)]_{\alpha \in \mathrm{CH}_N}$ by

$$\mathrm{F}_{\lambda,D}[g(\xi)]_{\xi \in \mathrm{CH}_N} = [\mathcal{F}[\ell_\lambda[g(\xi)]_{\xi \in \mathrm{CH}_N}](\alpha)]_{\alpha \in \mathrm{CH}_N}. \tag{33}$$

The degree D browses the values (32), so that various approximation spaces are considered. The regularization parameter λ browses the values

$$\lambda = 10^{-p}, \quad 1 \leq p \leq 8, \tag{34}$$

so that the matrix of (RLS) has not a huge condition number, as displayed in Figure 4. In each case, we compute the relative error on CH_N, and we keep the minimal one,

$$\epsilon_N[g] = \min_{\substack{D = 2N + \lceil \frac{iN}{4} \rceil,\ 0 \leq i \leq 4 \\ \lambda = 10^{-p},\ 1 \leq p \leq 8}} \left(\frac{\sum_{\alpha \in \mathrm{CH}_N} \left[\mathrm{F}_{\lambda,D}[g(\xi)]_{\xi \in \mathrm{CH}_N}(\alpha) - \mathcal{F}g(\alpha) \right]^2}{\sum_{\alpha \in \mathrm{CH}_N} \left[\mathcal{F}g(\alpha) \right]^2} \right)^{1/2}. \tag{35}$$

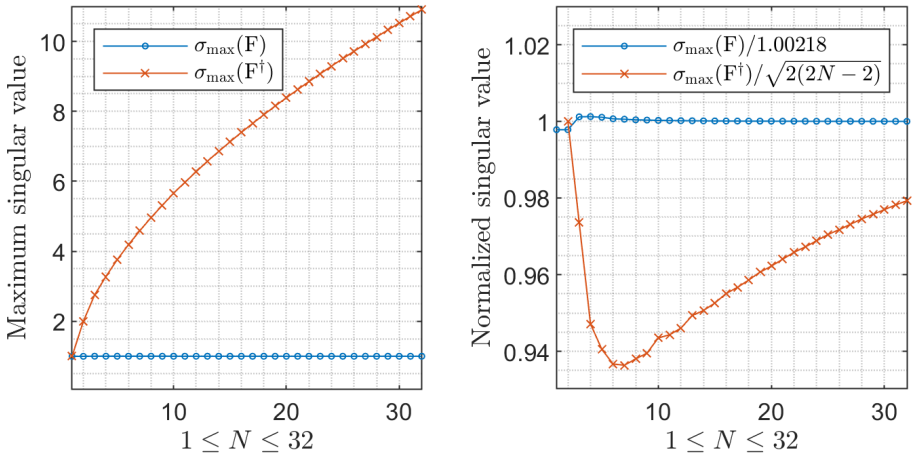

FIGURE 5. Stability constants associated to the discrete Funk transform F, and the pseudoinverse $\mathrm{F}^\dagger$. Left: the maximum singular values $\sigma_{\max}(\mathrm{F})$ and $\sigma_{\max}(\mathrm{F}^\dagger)$ are plotted in term of N. Right: the same singular values are plotted, but with "normalization" factors.

In order to compare with the error $\eta_N[g]$, we plot the ratio $\eta_N[g]/\epsilon_N[g]$ in Figure 3 (right panel). In most of the cases, the order of magnitude of this ratio is 1, which shows that the approximation $\mathrm{F}[g(\xi)]$ is as relevant as the "best" approximation $\mathrm{F}_{\lambda,D}[g(\xi)]$ (with the "best" (D,λ)). The main exception is the test function $g = g^{(-\infty)}$, for which the coefficients have a factorial decay. In this case, for $N = 4$, the ratio is about 10^2, so that the "best" $\mathrm{F}_{\lambda,D}[g(\xi)]$ is significantly better than $\mathrm{F}[g(\xi)]$, but if $N \ge 7$, the observed ratio is between 10^{-3} and 10^{-7} so that the result is significantly better for $\mathrm{F}[g(\xi)]$.

To conclude, the conditioning of (RLS) with $D \ge 2N$ cannot be significantly better than the conditioning of (LS) with $D = 2N - 2$. Furthermore, the accuracy of the Funk transform F is competitive with the accuracy of $\mathrm{F}_{\lambda,D}$ from (33), even if the degree $D \ge 2N$ and the parameter $\lambda \ge 0$ are "optimized". Therefore, it is not really worth considering regularized problems (RLS) with $D \ge 2N$ to define a discrete Funk transform on the Cubed Sphere. This is in line with our definition of F.

5.3. **Stability constants.** We investigate the stability of the discrete Funk transform F and its pseudoinverse $\mathrm{F}^\dagger$.

We compute the maximum singular value of F, resp. $\mathrm{F}^\dagger$, given by (26). We observe in Figure 5 that the transform F is very stable, since for every $N \ge 1$,

$$\sigma_{\max}(\mathrm{F}) \approx 1.00218.$$

Concerning the pseudoinverse, Figure 5 suggests a reasonable growth such as

$$\sigma_{\max}(\mathrm{F}^\dagger) \approx \sqrt{2(2N-2)}.$$

These observations are in agreement with the theoretical bounds (27), with $\operatorname{cond} A \le 1.2$ plotted in Figure 2.

5.4. **Funk transform of Gaussian models.** We study the accuracy of the discrete Funk transform on Gaussian models from dMRI.

We consider Gaussian models in the following form,

$$S(x) = \exp(-b\, x^{\intercal}\mathbf{D}x), \quad x \in \mathbb{S}^2, \tag{36}$$

where $b \ge 0$, and $\mathbf{D} \in \mathbb{R}^{3\times 3}$ is a symmetric positive definite matrix. Such models describe the dMRI signal S in Diffusion Tensor Imaging. The so-called *diffusion tensor* $\mathbf{D}$ models intrinsic diffusion properties of biological tissues. The parameter b is the so-called *b-value*, and is a parameter of the acquisition. The unit vector x, represents a *gradient direction*, and browses a hemispherical grid during the acquisition. Gaussian models such as (36) appear also in High

i	b_i [s/mm^2]	$\mathbf{D}_i$ [mm^2/s]	FA
1	1000	$10^{-6}\,\mathrm{diag}(300, 300, 300)$	0
2	1000	$10^{-6}\,\mathrm{diag}(300, 600, 900)$	0.46
3	1000	$10^{-6}\,\mathrm{diag}(300, 300, 1700)$	0.80
4	3000	$10^{-6}\,\mathrm{diag}(300, 300, 300)$	0
5	3000	$10^{-6}\,\mathrm{diag}(300, 600, 900)$	0.46
6	3000	$10^{-6}\,\mathrm{diag}(300, 300, 1700)$	0.80

TABLE 2. Parameters of the Gaussian signals (37). The anisotropy is measured by the fractional anisotropy (FA), defined in (38).

Angular Resolution Diffusion Imaging [11]. In this field, a weighted average of several Gaussian models can be introduced to model the signal from crossing fibers. The orientation of the fibers can be imaged using an Orientation Distribution Function, which is computed approximately as the Funk transform of the recorded signal S [12, 41]. Hence, it is crucial to be able to compute accurately the Funk transform of a Gaussian model, from a discrete set of values.

In this paper, we consider Gaussian signals

$$S_i(x) = \exp(-b_i\, x^\intercal \mathbf{D}_i x), \quad x \in \mathbb{S}^2, \quad 1 \leq i \leq 6. \tag{37}$$

The b-values b_i and the diffusion tensors $\mathbf{D}_i$ are defined in Table 2. Our values are inspired by the values from [12]. The b-value $b = 1000$ [s/mm^2] is an usual clinical value, whereas $b = 3000$ [s/mm^2] is considered as relatively high. For the diffusion tensors, we have chosen diagonal matrices $\mathbf{D}_i$, defined by the eigenvalues μ_1, μ_2, $\mu_3 > 0$. The matrix $\mathbf{D}_3$ has been found in the synthetic data generation in [12]. The other matrices have been defined as "variations" of this matrix, in order to obtain more or less anisotropy; see the last column of Table 2, where anisotropy is measured by means of the *fractional anisotropy* (FA),

$$\mathrm{FA} = \tfrac{1}{\sqrt{2}} \sqrt{\tfrac{(\mu_1-\mu_2)^2+(\mu_1-\mu_3)^2+(\mu_2-\mu_3)^2}{\mu_1^2+\mu_2^2+\mu_3^2}} \in [0, 1]. \tag{38}$$

Firstly, we assume that the (even) signal S_i is recorded on the Cubed Hemisphere CH_N, with $N \geq 1$ and $1 \leq i \leq 6$. We compute reference values $[\mathcal{F}[S_i](\alpha)]_{\alpha \in \mathrm{CH}_N}$ using trapezoidal rules[2]. Then, we compute the discrete Funk transform $\mathrm{F}[S_i(\xi)]_{\xi \in \mathrm{CH}_N}$. It approximates $[\mathcal{F}[S_i](\alpha)]_{\alpha \in \mathrm{CH}_N}$, with a relative error $\eta_N[S_i]$, where η_N is defined in (30). We have plotted these errors in Figure 6 (left panel) to evaluate the accuracy of the procedure. Overall, a fast convergence due to the smoothness of the Gaussian signals is observed. For the isotropic functions S_1 and S_4, the error is always zero (up to rounding errors), because S_1, $S_4 \in \mathcal{Y}_0 \subset \mathcal{Y}^{\mathrm{ev}}_{2N-2}$, so (21) applies. With S_2, S_5, and S_3, S_6, we observe that increasing the b-value induces a loss in accuracy; this is because a Gaussian becomes sharper with high b-values.

Secondly, we show that the orientation of the grid does not matter. For that purpose, we consider "rotations" of the signals S_i:

$$S_i(Q^\intercal \cdot) : x \mapsto S_i(Q^\intercal x) = \exp(-b\, x^\intercal\, Q \mathbf{D}_i Q^\intercal\, x),$$

where $Q \in \mathbb{R}^{3\times 3}$ is a random orthogonal matrix. The relative error of approximation of the Funk transform becomes $\eta_N[S_i(Q^\intercal \cdot)]$, and can be computed as before. For each function S_i, we repeat this procedure for 30 random orthogonal matrices Q, and we plot the maximum error

$$\max_Q \eta_N[S_i(Q^\intercal \cdot)] \tag{39}$$

[2]Here, an integral along a great circle $x \cdot \alpha = 0$ is an integral of a smooth 2π-periodic function over a period, so the trapezoidal rule converges exponentially to the true integral [40]. Therefore, we apply successive trapezoidal rules as follows. We start with an angular step $\frac{\pi}{8}$. We evaluate the associated trapezoidal rule; then, we divide the angular step by two, and we iterate. The iterations are stopped as soon as the relative increase of the value between two successive iterations is below the tolerance 10^{-13}.

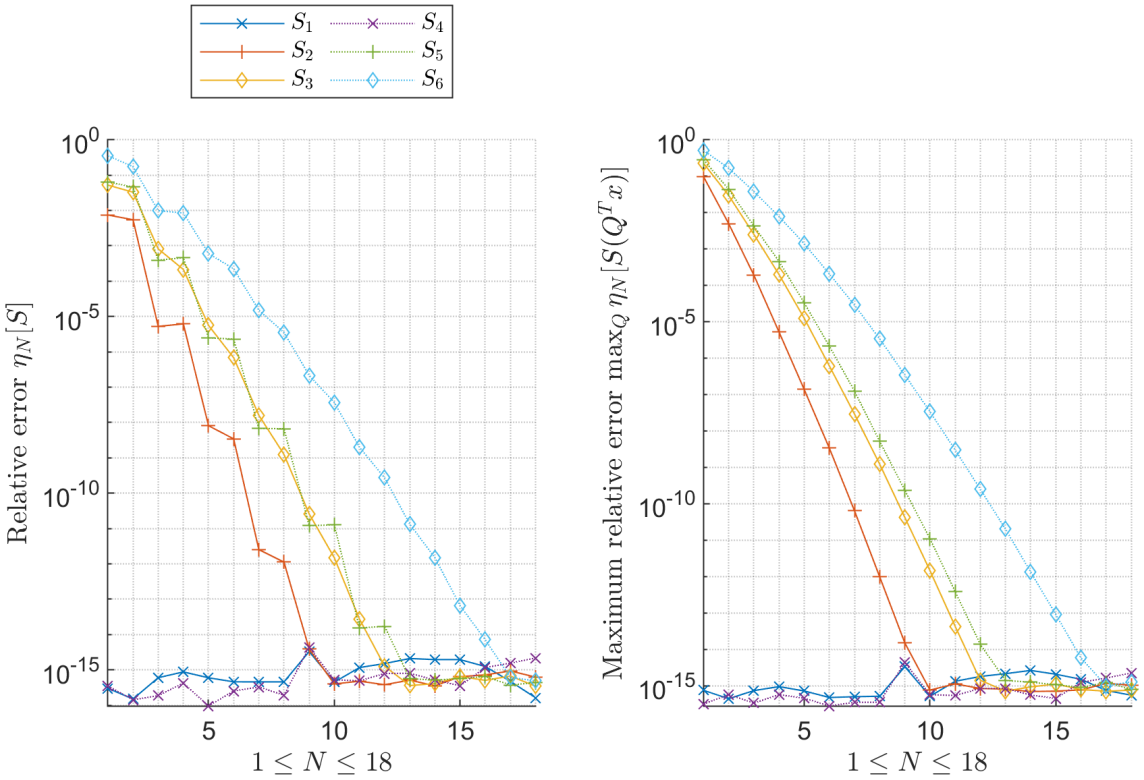

FIGURE 6. Accuracy of the discrete Funk transform for the Gaussian signals S_i defined in (37) and Table 6. Left: the discrete transform $\mathrm{F}[S_i(\xi)]_{\xi\in\mathrm{CH}_N}$ approximates $[\mathcal{F}[S_i](\xi)]_{\xi\in\mathrm{CH}_N}$ with relative error $\eta_N[S_i]$ defined in (30); $\eta_N[S_i]$ is plotted. Right: for any orthogonal matrix $Q \in \mathbb{R}^{3\times 3}$, the same procedure applied to the "rotated" Gaussian $S_i(Q^\intercal \cdot)$ results in a relative error $\eta_N[S_i(Q^\intercal\cdot)]$; we plot the maximum error (39), where Q scans a set of 30 random orthogonal matrices.

in Figure 6 (right panel). We obtain a similar conclusion than before, so that the conclusion does not depend on the orientation of the grid.

Thirdly, we investigate the effect of noise. We corrupt the signals as follows. We fix a value of N. For any $1 \leq i \leq 6$, for any $\sigma = 2^{-p}$, with $2 \leq p \leq 31$, we corrupt S_i, by a "speckle" noise and an additive noise with level σ:

$$S_i^\sigma(\xi) = |S_i(\xi)(1 + \sigma u(\xi)) + \sigma v(\xi)|, \quad \xi \in \mathrm{CH}_N,$$

where the $u(\xi)$, $v(\xi)$, are $6N^2 + 2$ independent realizations of the normal law $\mathcal{N}(0, 1)$. In this case, the relative error on the signal is given by

$$\left(\frac{\sum_{\xi\in\mathrm{CH}_N} [S_i(\xi) - S_i^\sigma(\xi)]^2}{\sum_{\xi\in\mathrm{CH}_N} S_i(\xi)^2} \right)^2. \tag{40}$$

We compute the discrete Funk transform $\mathrm{F}[S_i^\sigma(\xi)]$, which approximates $[\mathcal{F}S_i(\alpha)]$ with a relative error

$$\left(\frac{\sum_{\alpha\in\mathrm{CH}_N} [\mathrm{F}[S_i^\sigma(\xi)]_{\xi\in\mathrm{CH}_N}(\alpha) - \mathcal{F}S_i(\alpha)]^2}{\sum_{\alpha\in\mathrm{CH}_N} [\mathcal{F}S_i(\alpha)]^2} \right)^{1/2}. \tag{41}$$

In Figure 7, we have plotted the relative error (41) on the transform against the relative error (40) on the signal. Two values of N are considered. On the left, $N = 5$, so that the grid CH_N contains 76 points, and the approximation space is $\mathcal{Y}_8^{\mathrm{ev}}$. On the right, $N = 10$, so that the grid CH_N contains 301 points, and the approximation space is $\mathcal{Y}_{18}^{\mathrm{ev}}$. Roughly speaking, we observe that the relative error on the transform is the maximum between the relative error on the signal, and the relative error on the transform from the noise-free case (displayed in Figure 6). This result is in agreement with the stability constant of the transform F, $\sigma_{\max}(\mathrm{F}) \approx 1$ in Figure 5.

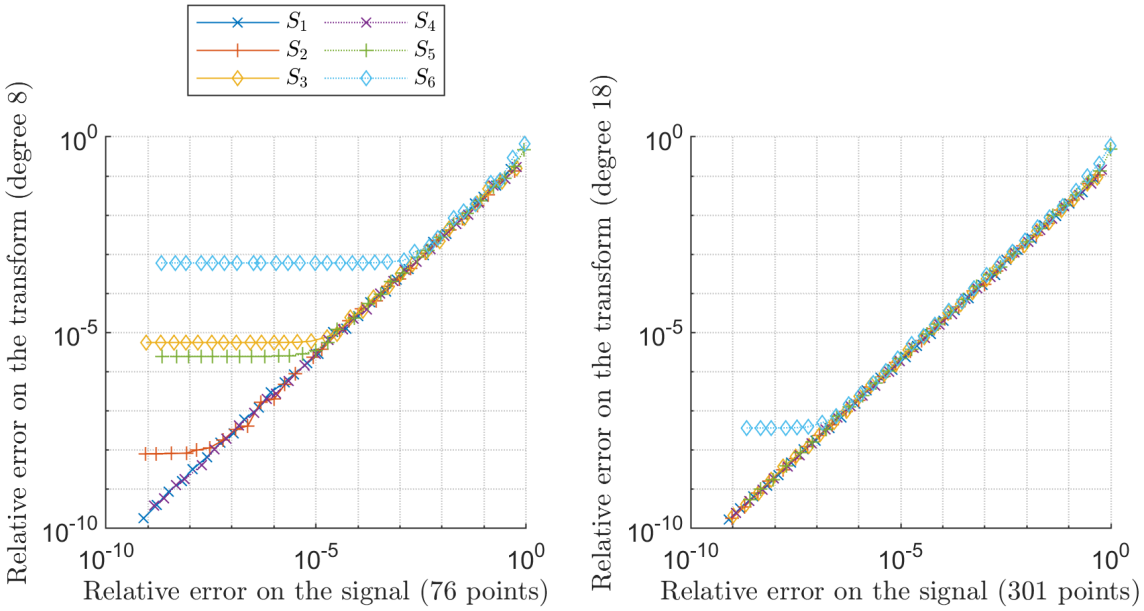

FIGURE 7. Accuracy of the discrete Funk transforms for Gaussian signals S_i corrupted by noise. The relative error (41) on the transform is plotted against the relative error (41) on the signal (logarithmic scale). Left: $N = 5$; right: $N = 10$.

To conclude, the Funk transform of Gaussian models can be accurately evaluated by the discrete transform F, and in a very stable way.

6. Conclusion

This paper has introduced a new discrete Funk transform F dedicated to the Cubed Sphere grid. It is based on a spectral method, and a least squares fitting that is tuned for this problem. It enjoys various theoretical properties. Interestingly, the same principle applied on the inverse Funk transform provides exactly the pseudoinverse $\mathrm{F}^\dagger$, so that the paper tackles simultaneously the inversion of F. Several numerical results show that the discrete transform F is relevant for numerical computation. Continuous Funk transforms can be accurately approximated by means of the discrete transform F. A remarkable property is that the transforms F and $\mathrm{F}^\dagger$ are stable, despite they are computed without any regularization.

This work opens new problems to be addressed in the future. There are still important theoretical questions. Proving that the Vandermonde matrix A from Definition 1 has full column rank (with a low condition number) is still open. Another point concerns the speed of convergence; our numerical results suggest to quantify the rate of convergence in Sobolev spaces. Concerning implementation aspects, writing a "fast" algorithm corresponding to F (or an approximation of F) is still to be done. To finish with, concerning the practice, comparing F with time-tested transforms on real experiments is a goal for further studies.

References

[1] C. An, X. Chen, I. H. Sloan, and R. S. Womersley. Regularized least squares approximations on the sphere using spherical designs. *SIAM Journal on numerical analysis*, 50(3):1513–1534, 2012.

[2] K. Atkinson and W. Han. *Spherical harmonics and approximations on the unit sphere: an introduction*, volume 2044. Springer Science & Business Media, 2012.

[3] J.-B. Bellet. Symmetry group of the equiangular cubed sphere. *Quarterly of Applied Mathematics*, 80:69–86, 2022.

[4] J.-B. Bellet, M. Brachet, and J.-P. Croisille. Interpolation on the Cubed Sphere with Spherical Harmonics. *https://hal.archives-ouvertes.fr/hal-03202236*, 2021. Under review (after minor revision).

[5] J.-B. Bellet, M. Brachet, and J.-P. Croisille. Quadrature and symmetry on the Cubed Sphere. *Journal of Computational and Applied Mathematics*, 409, 2022.

[6] J.-B. Bellet and J.-P. Croisille. Least Squares Spherical Harmonics Approximation on the Cubed Sphere. *https://hal.archives-ouvertes.fr/hal-03788836*, 2022. Under review.
[7] M. Brachet. *Schémas compacts hermitiens sur la Sphère: applications en climatologie et océanographie numérique*. PhD thesis, Université de Lorraine, 2018 (in French).
[8] M. Brachet and J.-P. Croisille. Spherical Shallow Water simulation by a cubed sphere finite difference solver. *Quarterly Journal of the Royal Meteorological Society*, 147(735):786–800, 2021.
[9] C. Chen and F. Xiao. Shallow water model on cubed-sphere by multi-moment finite volume method. *Journal of Computational Physics*, 227(10):5019–5044, 2008.
[10] S. Chevrot, R. Martin, and D. Komatitsch. Optimized discrete wavelet transforms in the cubed sphere with the lifting scheme—implications for global finite-frequency tomography. *Geophysical Journal International*, 191(3):1391–1402, 2012.
[11] M. Descoteaux. *High Angular Resolution Diffusion Imaging (HARDI)*, pages 1–25. John Wiley & Sons, Ltd, 2015.
[12] M. Descoteaux, E. Angelino, S. Fitzgibbons, and R. Deriche. Regularized, Fast, and Robust Analytical Q-Ball Imaging. *Magnetic Resonance in Medicine*, 58:497–510, 2007.
[13] M. Faham and H. Nasir. Weakly Orthogonal Spherical Harmonics in a Non-Polar Spherical Coordinates and its Application to Functions on Cubed-Sphere. *Sultan Qaboos University Journal for Science*, 17(2):200–213, 2012.
[14] P. Funk. Über Flächen mit lauter geschlossenen geodätischen Linien. *Mathematische Annalen*, 1913.
[15] G. H. Golub and C. F. Van Loan. *Matrix computations*. The Johns Hopkins University Press, third edition, 1996.
[16] P. C. Hansen. *Rank-deficient and discrete ill-posed problems: numerical aspects of linear inversion*, volume 4. Siam, 2005.
[17] R. Hielscher and M. Quellmalz. Reconstructing a function on the sphere from its means along vertical slices. *Inverse Problems and Imaging*, 10(3):711–739, 2016.
[18] Y. Hristova, S. Moon, and D. Steinhauer. A radon-type transform arising in photoacoustic tomography with circular detectors: spherical geometry. *Inverse Problems in Science and Engineering*, 24(6):974–989, 2016.
[19] L. Ivan, H. De Sterck, S. A. Northrup, and C. P. T. Groth. Multi-dimensional finite-volume scheme for hyperbolic conservation laws on three-dimensional solution-adaptive cubed-sphere grids. *Journal of Computational Physics*, 255:205–227, 2013.
[20] J. H. Jensen, G. R. Glenn, and J. A. Helpern. Fiber Ball Imaging. *NeuroImage*, 124:824–833, 2016.
[21] B. A. Jones, G. H. Born, and G. Beylkin. Comparison of the Cubed-Sphere Gravity Model with the Spherical Harmonics. *Journal of Guidance, Control, and Dynamics*, 33(2):415–425, 2010.
[22] H.-G. Kang and H.-B. Cheong. An efficient implementation of a high-order filter for a cubed-sphere spectral element model. *Journal of Computational Physics*, 332:66–82, 2017.
[23] S. Kazantsev. Funk–Minkowski transform and spherical convolution of Hilbert type in reconstructing functions on the sphere. *Siberian Electronic Mathematical Reports*, 15:1630–1650, 2018.
[24] D. Lee and A. Palha. A mixed mimetic spectral element model of the rotating shallow water equations on the cubed sphere. *Journal of Computational Physics*, 375:240–262, 2018.
[25] A. K. Louis, M. Riplinger, M. Spiess, and E. Spodarev. Inversion algorithms for the spherical radon and cosine transform. *Inverse Problems*, 27(3):035015, 2011.
[26] J. L. McGregor. Semi-Lagrangian Advection on Conformal-Cubic Grids. *Monthly Weather Review*, 124(6):1311–1322, 1996.
[27] R. D. Nair, S. J. Thomas, and R. D. Loft. A Discontinuous Galerkin Transport Scheme on the Cubed Sphere. *Monthly Weather Review*, 133(4):814–828, 2005.
[28] R. J. Purser. Möbius Net Cubed-Sphere Gnomonic Grids. *Office note, National Meteorological Center (U.S.)*, 496, 2018.
[29] R. J. Purser and M. Rančić. Smooth quasi-homogeneous gridding of the sphere. *Quarterly Journal of the Royal Meteorological Society*, 124(546):637–647, 1998.
[30] R. J. Purser and M. Tong. A minor modification of the gnomonic cubed-shaped sphere grid that offers advantages in the context of implementing moving hurricane nests. *Office note, National Centers for Environmental Prediction (U.S.)*, 486, 2017.
[31] W. M. Putman. *Development of the finite-volume dynamical core on the cubed-sphere*. PhD thesis, The Florida State University, 2007.
[32] M. Quellmalz. A generalization of the Funk–Radon transform. *Inverse Problems*, 33(3):035016, 2017.
[33] M. Rančić, R. J. Purser, and F. Mesinger. A global shallow-water model using an expanded spherical cube: Gnomonic versus conformal coordinates. *Quarterly Journal of the Royal Meteorological Society*, 122(532):959–982, 1996.
[34] M. Rančić, R. J. Purser, D. Jović, R. Vasic, and T. Black. A Nonhydrostatic Multiscale Model on the Uniform Jacobian Cubed Sphere. *Monthly Weather Review*, 145(3):1083–1105, 2017.
[35] C. Ronchi, R. Iacono, and P. S. Paolucci. The "cubed sphere": a new method for the solution of partial differential equations in spherical geometry. *Journal of Computational Physics*, 124(1):93–114, 1996.

[36] J. A. Rossmanith. A wave propagation method for hyperbolic systems on the sphere. *Journal of Computational Physics*, 213(2):629–658, 2006.

[37] B. Rubin. Inversion formulas for the spherical Radon transform and the generalized cosine transform. *Advances in Applied Mathematics*, 29(3):471–497, 2002.

[38] R. Sadourny. Conservative finite-difference approximations of the primitive equations on quasi-uniform spherical grids. *Monthly Weather Review*, 100(2):136–144, 1972.

[39] S. J. Thomas, J. M. Dennis, H. M. Tufo, and P. F. Fischer. A Schwarz preconditioner for the cubed-sphere. *SIAM Journal on Scientific Computing*, 25(2):442–453, 2003.

[40] L. N. Trefethen and J. A. C. Weideman. The Exponentially Convergent Trapezoidal Rule. *SIAM Review*, 56(3):385–458, 2014.

[41] D. S. Tuch. Q-Ball Imaging. *Magnetic Resonance in Medicine*, 52:1358–1372, 2004.

[42] P. A. Ullrich, P. H. Lauritzen, and C. Jablonowski. Some considerations for high-order 'incremental remap'-based transport schemes: edges, reconstructions, and area integration. *International Journal for Numerical Methods in Fluids*, 71(9):1131–1151, 2013.

[43] C. E. Yarman and B. Yazici. Inversion of Circular Averages using the Funk Transform. In *2007 IEEE International Conference on Acoustics, Speech and Signal Processing - ICASSP '07*, volume 1, pages I–541–I–544, 2007.

[44] G. Zangerl and O. Scherzer. Exact reconstruction in photoacoustic tomography with circular integrating detectors II: Spherical geometry. *Mathematical Methods in the Applied Sciences*, 33(15):1771–1782, 2010.

Université de Lorraine, CNRS, IECL, F-57000 Metz, France
Email address: jean-baptiste.bellet@univ-lorraine.fr